Editors' Suggestion

Topology-Controlled Photonic Cavity Based on the Near-Conservation of the Valley Degree of Freedom

Yandong Li,[1,*] Yang Yu,[1] Fengyu Liu,[1,2] Baile Zhang,[3,4] and Gennady Shvets[1,†]
[1]School of Applied and Engineering Physics, Cornell University, Ithaca, New York 14853, USA
[2]School of Physics, Nankai University, Tianjin 300071, China
[3]Division of Physics and Applied Physics, School of Physical and Mathematical Sciences, Nanyang Technological University, 21 Nanyang Link, Singapore 637371, Singapore
[4]Centre for Disruptive Photonic Technologies, The Photonics Institute, Nanyang Technological University, 50 Nanyang Avenue, Singapore 639798, Singapore

(Received 20 January 2020; accepted 23 September 2020; published 18 November 2020)

We demonstrate a novel path to localizing topologically nontrivial photonic edge modes along their propagation direction. Our approach is based on the near-conservation of the photonic valley degree of freedom associated with valley-polarized edge states. When the edge state is reflected from a judiciously oriented mirror, its optical energy is localized at the mirror surface because of an extended time delay required for valley index flipping. The degree of energy localization at the resulting topology-controlled photonic cavity is determined by the valley-flipping time, which is in turn controlled by the geometry of the mirror. Intuitive analytic descriptions of the "leaky" and closed topology-controlled photonic cavities are presented, and two specific designs—one for the microwave and the other for the optical spectral ranges—are proposed.

DOI: 10.1103/PhysRevLett.125.213902

The reflection of a photon from a perfect mirror is one of the simplest and most fundamental phenomena in optics. Despite its simplicity, this phenomenon can be used to build one of the most important photonic components, a Fabry-Pérot cavity, by placing two parallel mirrors, separated by a finite distance L, along the photon's path. Electromagnetic waves with the wavelengths λ_N satisfying a constructive interference condition $L = (N - 1/2)\lambda_N$ are trapped in such a cavity in the form of a standing wave with N maxima (antinodes) uniformly spaced between the mirrors. The energy confinement volume of every electromagnetic eigenmode is thus equal to that of a conventional cavity. This can be intuitively understood by noting that the photons spend most of their time traveling between the mirrors. In this Letter, we pose, and affirmatively answer, the following question: can we design an optical cavity from a novel perspective of manipulating the reflection time of a photon from the cavity mirror? If a photon can "stick" to the mirror for a long time, i.e., τ_{refl}, which is much longer than the time required for it to propagate the distance between two adjacent antinodes inside the Fabry-Pérot cavity, $T_{\mathrm{FP}} \sim \lambda_N/(2v_g)$, then the optical energy could be expected to strongly localize near the mirror.

The approach presented in this Letter uses photonic topological insulators (PTIs) [1] to engineer the reflection time τ_{refl}. One key feature of topological photonics [2–11] is the existence of robust unidirectional edge or kink states propagating either along the PTI edges or along the interface between two topologically distinct PTIs. Upon encountering photonic defects, such robust modes circumvent them rather than suffer back-reflection [1–8,12–17]. The propagation direction of topologically robust edge (kink) (TREK) states is typically linked to a topologically conserved quantity, such as the Chern, spin-Chern, or valley-Chern indices (C, C_s, or C_v, respectively). While $C = 0$ for any time-reversal invariant photonic structure, its crystalline symmetries can produce discrete degrees of freedom (DOFs) such as spin and valley [16–21] and endow the structure with nonvanishing topological indices C_s and C_v. Therefore, backscattering a TREK state requires breaking the bulk topological order of a PTI and changing the corresponding topological index [9,11].

In this Letter, we concentrate on the controllable flipping of the valley DOF [22–24] achieved through a symmetry-breaking termination of a valley photonic crystal (VPC). The existence and robustness of valley-polarized TREK states have been experimentally demonstrated across the electromagnetic spectrum: from microwave to optical frequencies [19,25]. A number of novel optical devices based on VPCs have been proposed, including delay lines [18], quantum optical platforms [26], and nanoscale topological waveguides [27]. When a valley-polarized TREK state is reflected by a terminating mirror due to the reversal of its valley DOF, if the effective reflection time τ_{refl} is sufficiently long, then the near-conservation of the valley DOF can result in a subwavelength topology-controlled photonic cavity (TCPC) near the mirror. Furthermore,

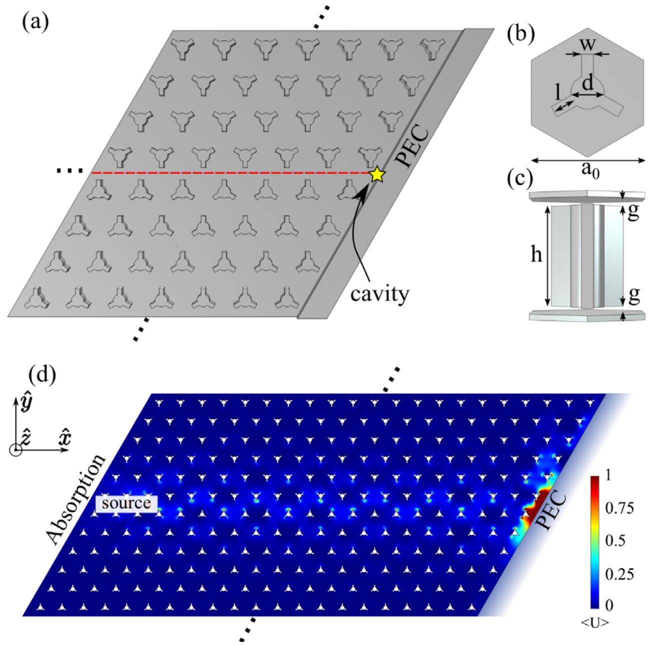

FIG. 1. (a) A "leaky" TCPC based on the near-conservation of the valley DOF in a mirror-terminated photonic structure. TREK states are supported by a domain wall (red horizontal line) between two VPCs with opposite C_v. (b) Top and (c) side views and geometry definitions of the unit cell. (d) Energy from an excited TREK state is localized at the cavity for $\omega = 0.75(2\pi c/a_0)$. Color: time-averaged energy density. Dimensions: $l = 0.12a_0$, $w = 0.06a_0$, $d = 0.2a_0$, $g = 0.03a_0$, and $h = 0.94a_0$. The sketches in (a),(b),(c) are not to scale.

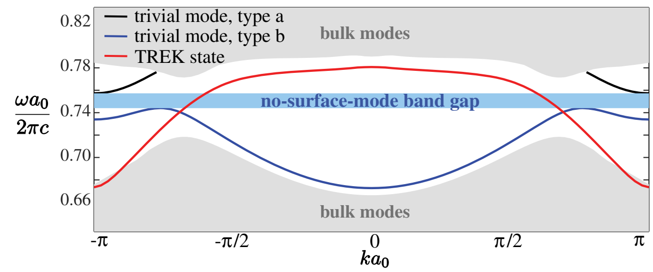

FIG. 2. Dispersion bands of the TE-polarized TREK state (red line) and trivial surface modes (black and blue lines). The wave number k is along the domain wall for the TREK state and along the PEC mirror for the trivial modes. Black lines: type a trivial mode, propagating downward [direction $-\hat{x}/2 - \sqrt{3}\hat{y}/2$ in Fig. 1(d)] along the mirror. Blue line: type b trivial mode, propagating upward (opposite to type a) along the mirror. Only the TREK state can propagate inside the no-surface-mode band gap. Structure parameters: same as in Fig. 1.

we demonstrate that a nonmetallic photonic crystal (PhC) extends this concept to optical frequencies.

The first example of a TCPC is a structure comprising a triangular lattice of tripod-shaped perfect electric conducting (PEC) pillars [17] symmetrically inserted between two parallel plates separated by the distance $h_0 = h + 2g$ [shown in Fig. 1(a), (b), (c)]. The structure contains a domain wall separating two topologically nontrivial VPCs that are mirror reflections of each other about the x–z plane (where the x axis is chosen along the nearest-neighbor direction of the lattice). Therefore, the two VPCs have opposite valley-Chern indices $C_v = \pm 1/2$ [18], and the resulting domain wall supports $K(K')$-valley-polarized TREK states propagating along the forward (backward) directions [17–19]. The VPC supports electromagnetic modes whose in-plane electric field components $E_{x,y}$ are either symmetric [transverse electric (TE) polarized] or antisymmetric [transverse magnetic (TM) polarized] with respect to the $z = h_0/2$ mirror symmetry plane [28]. In what follows, we focus on the TE TREK state whose dispersion band $\omega_{\mathrm{TREK}}(k)$ is plotted in Fig. 2 as a red line.

The structure is terminated by a PEC mirror producing intervalley scattering at a rate $\tau_{\mathrm{refl}}^{-1}$, which, we assume, is determined by its shape and orientation. As an example, we consider a straight mirror oriented at 60° with respect to the propagation direction of the K-valley ($k \sim 4\pi/3a$) TREK state. When a forward-propagating TREK state encounters the mirror, it has three distinct scattering channels. The first and the second channels involve scattering either up or down the mirror-VPC interface into topologically trivial surface modes. The dispersion curves of the trivial modes are plotted in Fig. 2 as black (blue) lines corresponding to downward (upward) modes labeled as type $a(b)$. The trivial modes are localized near the terminating mirror (see the Supplemental Material [29]). Because the trivial surface modes do not span the entire band gap, there exists a frequency range labeled as a no-surface-mode band gap shown in Fig. 2. When a TE-polarized TREK state is inside the no-surface-mode band gap, it cannot scatter into either of the two trivial modes. The third scattering mechanism is back-scattering, and it requires the reversal of the mode's valley index from K to K'. Therefore, the valley-flipping rate is identical to the decay rate of the "leaky" VPC-based TCPC.

Previous studies revealed that the rate of valley-flipping depends on the geometry of the perturbations [18,19,21]. For example, perturbations along the principal axes of the lattice (the so-called zigzag directions) significantly suppress intervalley scattering. On the other hand, perturbations along the orthogonal (armchair) directions produce much higher rates of intervalley scattering. It is expected that the zigzag orientation of the PEC mirror chosen in Fig. 1(a) should minimize (albeit not entirely eliminate) valley flipping. The evanescent nature of the TREK states along the direction normal to that of their propagation is responsible for the residual rate of valley flipping (see the Supplemental Material [29] for the detailed calculation).

Within the no-surface-mode band gap, this "leaky" TCPC can be analytically described as a resonator at an abruptly terminated end [44–47] of a topologically robust port. The driven Lorentzian response of the resonator to a time-harmonic input signal with frequency $\omega \equiv \omega_0 + \Delta\omega$ is

$$|A|^2 = |s^+|^2 \frac{2\gamma}{(\omega - \omega_0)^2 + \gamma^2}, \tag{1}$$

where A and s^+ are the complex-valued mode amplitude and incoming wave amplitude, and ω_0 and γ are the resonator eigenfrequency and decay rate (see the Supplemental Material [29] for details). We extract ω_0 and $\gamma \equiv \tau_{\rm refl}^{-1}$ of the VPC-based TCPC shown in Fig. 1 by numerically fitting the simulated energy content inside the cavity as a function of $\Delta\omega$ (see the Supplemental Material [29]). The extracted cavity parameters are $\omega_0 \approx 0.75(2\pi c/a_0)$ and $\gamma \approx 3.1 \times 10^{-3}(2\pi c/a_0)$. The reflection time is hence $\tau_{\rm refl} \approx 51.3(a_0/c)$.

Note that $\tau_{\rm refl} \gg T_{\rm FP} \sim a_0/v_g \approx 2.9(a_0/c)$, where a_0 is the lattice constant and v_g is the group velocity of the TREK state. This result confirms our initial conjecture that a terminating mirror of the zigzag type indeed presents a weak valley-flipping perturbation to a propagating TREK state, delaying the reflection and resulting in energy confinement. The "leaky" resonator with a Q factor equal to $Q \equiv \omega_0/(2\gamma) \approx 121$ is based on the near-conservation of the valley DOF.

The near-conservation of the valley DOF can also be used for designing closed Fabry-Pérot resonators. An example of such a cavity terminated by PEC mirrors on both ends of the domain wall is shown in Fig. 3. Below we demonstrate that the near-conservation of the valley DOF produces electromagnetic mode structures that can be very distinct from those in conventional Fabry-Pérot resonators. Specifically, if $\tau_{\rm refl} \gg T_{\rm FP}$ is satisfied, then the modes are strongly confined at the surfaces of the terminating mirrors. On the other hand, when this condition is violated, the modes are uniformly distributed between the mirrors, as expected for a Fabry-Pérot resonator.

To describe the closed TCPC, we develop an analytic one-port-two-cavity model schematically illustrated in Fig. 3(b) and described by the following coupled differential equations for the complex-valued cavity mode amplitudes A and B [28,48–50]:

$$\frac{dA}{dt} = -(i\omega_0 + \gamma)A + K_a s_a^+,$$
$$\frac{dB}{dt} = -(i\omega_0 + \gamma)B + K_b s_b^+, \tag{2}$$

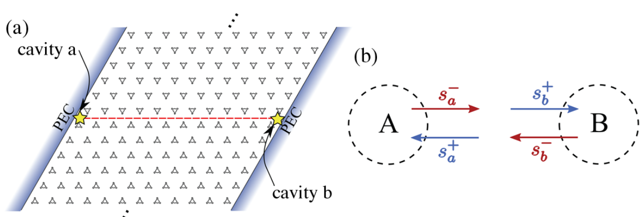

FIG. 3. (a) A VPC-based TCPC terminated by PEC reflectors on both ends. (b) The corresponding one-port-two-cavity model of the TCPC.

where the incoming (outgoing) wave amplitude $s_{a(b)}^{+(-)}$ coupled to cavity $a(b)$ is calculated as

$$s_a^- = C_a s_a^+ + D_a A \quad \text{and} \quad s_b^- = C_b s_b^+ + D_b B. \tag{3}$$

Here, $K_{a,b}$ and $D_{a,b}$ are the coupling-in and coupling-out coefficients of cavities a and b, respectively, and $C_{a,b}$ are the corresponding scattering coefficients. From the symmetric orientation of the two terminating mirrors, we further conclude that the two cavities are identical and therefore have the same eigenfrequency ω_0 and decay rate γ, as well as identical scattering and coupling coefficients: $D_a = D_b \equiv D$, $K_a = K_b \equiv K$, and $C_a = C_b \equiv C$. In the absence of nonradiative losses, energy conservation and time-reversal symmetry impose the following constraints [49,50]: $D^\dagger D = 2\gamma$, $K = D$, and $CD^* = -D$. Without loss of generality, we set $K = D = \sqrt{2\gamma}$ and $C = -1$. The only remaining relation is between the outgoing wave from cavity $b(a)$ and the incoming wave into cavity $a(b)$. Accounting for the phase shift $\alpha = -2\pi(L/\lambda)$ accumulated along the path of the TREK state, the following relations are obtained: $s_a^+ = e^{i\alpha} s_b^-$ and $s_b^+ = e^{i\alpha} s_a^-$, where the negative sign of α is due to the negative index of the TREK state.

The eigenfrequencies of the symmetric and antisymmetric eigenmodes of the cavity can be found analytically (see the Supplemental Material [29] for mode classification and analytic details):

$$\omega_{\rm sy} = \omega_0 - \gamma \tan(\alpha/2) \quad \text{and} \quad \omega_{\rm an} = \omega_0 + \gamma \cot(\alpha/2), \tag{4}$$

where $\omega_{\rm sy(an)}$ are the eigenfrequencies of the symmetric (antisymmetric) eigenmodes.

This analytic model reveals a characteristic feature of the symmetric and antisymmetric modes: the ratio of the energy inside the cavities, $U_{\rm cav} \propto (|A|^2 + |B|^2)$, to the energy per antinode inside the topological waveguide, $U_{\rm wg} \propto \sum_{i=a,b} |s_i|^2 a_0/v_g$, is inversely proportional to the decay rate γ:

$$\frac{U_{\rm cav}^{\rm sy}}{U_{\rm wg}} \propto \frac{2\cos^2(\alpha/2)}{\gamma a_0/v_g} \quad \text{and} \quad \frac{U_{\rm cav}^{\rm an}}{U_{\rm wg}} \propto \frac{2\sin^2(\alpha/2)}{\gamma a_0/v_g}. \tag{5}$$

Our model predicts that energy is more localized in the cavities when the decay rate γ is smaller [see Fig. 5(c), (d) and the Supplemental Material [29] for details].

As concluded previously, the decay rate from the cavity is the rate of valley flipping at the PEC boundary, which strongly depends on the type of geometry (zigzag or armchair) of the termination. Therefore, we expect that the energy is mostly localized in the cavities with zigzag terminations, whereas, with armchair terminations, the energy is mostly stored inside the waveguide. This intuitive conclusion is confirmed by the result of COMSOL simulations of the cavity eigenmodes inside the two types

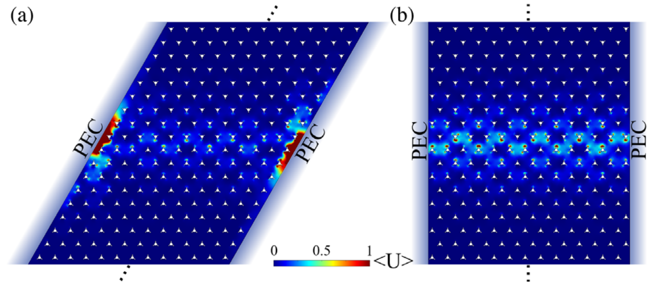

FIG. 4. Examples of the time-averaged energy distributions of the eigenmodes of the TCPC. (a) With zigzag terminations, energy is mostly localized in the two cavities. (b) With armchair terminations, energy is distributed in the waveguide. Horizontal cavity length is $L = 13a_0$ for both cases.

of platforms shown in Fig. 4: the zigzag-oriented mirrors in Fig. 4(a) indeed produce much stronger field localization than the armchair-oriented mirrors in Fig. 4(b).

Next, we check the applicability of the analytic model to the realistic system shown in Fig. 4. By varying the path length of the TREK state from $L_{\min} = 6a_0$ to $L_{\max} = 21a_0$ (with $\Delta L = a_0$ per increment), we vary the phase delay α. For each length $L_{\min} \leq L \leq L_{\max}$ of the topological channel, we extract the frequencies $\omega_{\mathrm{sy,an}}$ of the symmetric and antisymmetric eigenmodes from COMSOL and calculate γ by fitting the simulation results to Eq. (4) (Fig. 5). We have found that $\gamma_{\mathrm{zig}} \approx 6.4 \times 10^{-3}(2\pi c/a_0)$ for the zigzag termination and $\gamma_{\mathrm{arm}} \approx 3.0 \times 10^{-1}(2\pi c/a_0)$ for the armchair termination.

Remarkably, the zigzag termination delays the reflection for an extra time of $\tau = 1/\gamma_{\mathrm{zig}} - 1/\gamma_{\mathrm{arm}} \approx 24.4(a_0/c)$ compared to the armchair termination. Such a long delay is consistent with the high Q value of the leaky single-mirror TCPC described earlier. It is also in agreement with the time delay calculated by numerically processing the back-reflected wave of COMSOL simulation (see the Supplemental Material [29]). Moreover, it is possible to increase the reflection time by further suppressing the intervalley scattering at the PEC surface through optimizing the geometrical detail of the zigzag termination (see the Supplemental Material [29]). We observe the following hierarchy of the timescales: $\tau_{\mathrm{refl,zig}} \gg T_{\mathrm{FP}} \gg \tau_{\mathrm{refl,arm}}$. Also, for the armchair termination, the possible phase shifts α are restricted to $\alpha \approx 2\pi N$ for symmetric or $\alpha \approx 2\pi(N + 1/2)$ for antisymmetric modes (N is an integer number). These conclusions are confirmed by Fig. 5(b). The large valley-flipping rate at the armchair termination makes the reflection happen almost instantaneously, thereby restoring all conventional properties of a Fabry-Pérot cavity. These phenomena are also observed for TM polarization (see the Supplemental Material [29]).

Furthermore, we demonstrate that the TCPC concept can be readily extended to optical frequencies by using all-dielectric VPCs [18] and replacing metallic mirrors with their PhC counterparts. The dispersion of the trivial mode

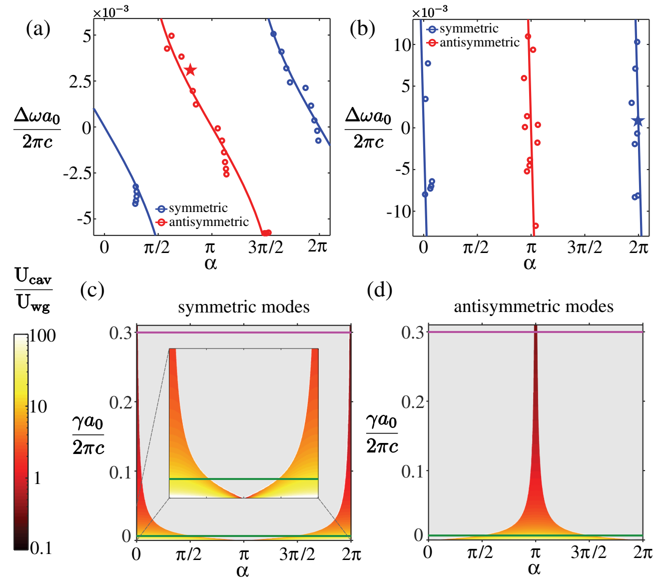

FIG. 5. (a),(b) Symmetric and antisymmetric eigenmodes data of the TCPC with (a) zigzag terminations and (b) armchair terminations. The circles are the numerical results from COMSOL; the lines are the analytic results from the coupled mode theory; the data points labeled by stars are related to the field profiles shown in Fig. 4. (c),(d) The ratios between the amounts of energy stored in the two cavities and the topological waveguide for (c) symmetric modes and (d) antisymmetric modes. Green lines represent $\gamma_{\mathrm{zig}}a_0/(2\pi c)$; magenta lines represent $\gamma_{\mathrm{arm}}a_0/(2\pi c)$. Only the solutions close to the center of the no-surface-mode band gap, i.e., $\omega_0 - \Delta\omega < \omega < \omega_0 + \Delta\omega$, are plotted, where $\omega_0 = 0.75(2\pi c/a_0)$ and $\Delta\omega = 0.01\omega_0$. The gray regions represent the combinations of γ and α corresponding to frequencies outside of that range, determined by Eq. (4).

along the VPC-PhC interface (see Supplemental Material [29]) defines the band gap, inside which no energy can leak through the interface. Therefore, when a TREK state encounters the interface, its reflection is delayed by the valley-flipping time, and its optical energy is concentrated at the junction between the two VPCs and the terminating trivial PhC (Fig. 6). Recent experimental developments in fabricating and characterizing all-dielectric topological

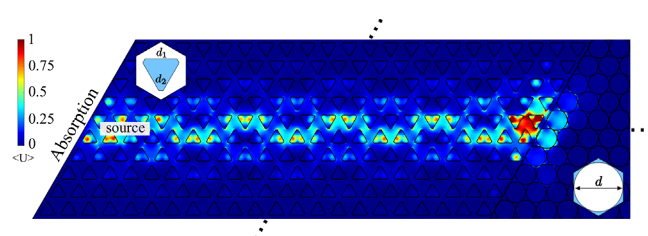

FIG. 6. An all-dielectric TCPC. Energy from an excited TREK state is localized at the cavity. The VPC region is formed by triangular Si rods; the trivial PhC region is a Si slab with arrayed holes. Color: time-averaged energy density. Frequency corresponds to $\omega = 0.43(2\pi c/a_0)$. $d_1 = 0.64a_0$, $d_2 = 0.09a_0$, $d = 0.98a_0$, and $\varepsilon_{\mathrm{Si}} = 13$.

VPCs [25,26,51] make us optimistic about near-future prospects for realizing optical TCPCs and using them for a variety of quantum optics applications [52–54].

In conclusion, we have demonstrated the localization of topologically robust edge (kink) states based on the near-conservation of the valley DOF. Distinct from conventional waveguide-cavity systems, the topologically nontrivial waveguide directly abuts the TCPC. The coupling rate between the TCPC and the topological waveguide is determined by the valley-index-flipping rate and can be controlled through perturbing the termination (see the Supplemental Material [29] for further discussions). Additionally, no time-reversal symmetry breaking is required. Unlike nanoplasmonic localization achieved through adiabatic tapering [55], the proposed approach does not require an extended tapering region. An all-dielectric realization of the TCPC is proposed using a combination of topologically trivial and nontrivial photonic crystals. We expect that the development of nonlinear and quantum optical devices and technologies will benefit from the TCPC concept.

This work was supported by Army Research Office under Grant No. W911NF-16-1-0319, by the National Science Foundation (NSF) under Grant No. DMR-1741788, and by the Cornell Center for Materials Research with funding from the NSF MRSEC program (DMR-1719875). Y. L. was supported in part by Cornell Graduate School Fellowship. F. L. acknowledges financial support from the Pilot Scheme of Talent Training in Basic Sciences (Boling Class of Physics, Nankai University). The authors would like to thank Minwoo Jung, Haoran Xue, and Ran Gladstone for their helpful discussions.

*Corresponding author.
yl2695@cornell.edu
†Corresponding author.
gshvets@cornell.edu

[1] A. B. Khanikaev, S. Hossein Mousavi, W.-K. Tse, M. Kargarian, A. H. MacDonald, and G. Shvets, Nat. Mater. **12**, 233 (2013).
[2] F. D. M. Haldane and S. Raghu, Phys. Rev. Lett. **100**, 013904 (2008).
[3] S. Raghu and F. D. M. Haldane, Phys. Rev. A **78**, 033834 (2008).
[4] Z. Wang, Y. D. Chong, J. D. Joannopoulos, and M. Soljačić, Phys. Rev. Lett. **100**, 013905 (2008).
[5] Z. Wang, Y. D. Chong, J. D. Joannopoulos, and M. Soljačić, Nature (London) **461**, 772 (2009).
[6] M. Hafezi, E. A. Demler, M. D. Lukin, and J. M. Taylor, Nat. Phys. **7**, 907 (2011).
[7] M. Hafezi, S. Mittal, J. Fan, A. Migdall, and J. M. Taylor, Nat. Photonics **7**, 1001 (2013).
[8] M. C. Rechtsman, J. M. Zeuner, Y. Plotnik, Y. Lumer, D. Podolsky, F. Dreisow, S. Nolte, M. Segev, and A. Szameit, Nature (London) **496**, 196 (2013).
[9] L. Lu, J. D. Joannopoulos, and M. Soljačić, Nat. Photonics **8**, 821 (2014).
[10] A. B. Khanikaev and G. Shvets, Nat. Photonics **11**, 763 (2017).
[11] T. Ozawa, H. M. Price, A. Amo, N. Goldman, M. Hafezi, L. Lu, M. C. Rechtsman, D. Schuster, J. Simon, O. Zilberberg, and I. Carusotto, Rev. Mod. Phys. **91**, 015006 (2019).
[12] Y. D. Chong, X.-G. Wen, and M. Soljačić, Phys. Rev. B **77**, 235125 (2008).
[13] K. Fang, Z. Yu, and S. Fan, Nat. Photonics **6**, 782 (2012).
[14] W.-J. Chen, S.-J. Jiang, X.-D. Chen, B. Zhu, L. Zhou, J.-W. Dong, and C. T. Chan, Nat. Commun. **5**, 5782 (2014).
[15] V. G. Sala, D. D. Solnyshkov, I. Carusotto, T. Jacqmin, A. Lemaître, H. Terças, A. Nalitov, M. Abbarchi, E. Galopin, I. Sagnes, J. Bloch, G. Malpuech, and A. Amo, Phys. Rev. X **5**, 011034 (2015).
[16] T. Ma, A. B. Khanikaev, S. H. Mousavi, and G. Shvets, Phys. Rev. Lett. **114**, 127401 (2015).
[17] T. Ma and G. Shvets, Phys. Rev. B **95**, 165102 (2017).
[18] T. Ma and G. Shvets, New J. Phys. **18**, 025012 (2016).
[19] F. Gao, H. Xue, Z. Yang, K. Lai, Y. Yu, X. Lin, Y. Chong, G. Shvets, and B. Zhang, Nat. Phys. **14**, 140 (2018).
[20] J.-W. Dong, X.-D. Chen, H. Zhu, Y. Wang, and X. Zhang, Nat. Mater. **16**, 298 (2017).
[21] J. Noh, S. Huang, K. P. Chen, and M. C. Rechtsman, Phys. Rev. Lett. **120**, 063902 (2018).
[22] D. Xiao, W. Yao, and Q. Niu, Phys. Rev. Lett. **99**, 236809 (2007).
[23] W. Yao, D. Xiao, and Q. Niu, Phys. Rev. B **77**, 235406 (2008).
[24] D. Xiao, G.-B. Liu, W. Feng, X. Xu, and W. Yao, Phys. Rev. Lett. **108**, 196802 (2012).
[25] M. I. Shalaev, W. Walasik, A. Tsukernik, Y. Xu, and N. M. Litchinitser, Nat. Nanotechnol. **14**, 31 (2019).
[26] S. Barik, A. Karasahin, S. Mittal, E. Waks, and M. Hafezi, Phys. Rev. B **101**, 205303 (2020).
[27] M. Jung, Z. Fan, and G. Shvets, Phys. Rev. Lett. **121**, 086807 (2018).
[28] J. D. Joannopoulos, S. G. Johnson, J. N. Winn, and R. D. Meade, *Photonic Crystals: Molding the Flow of Light* (Princeton University Press, Princeton, NJ, 2008).
[29] See Supplemental Material, which includes Refs. [30–43], at http://link.aps.org/supplemental/10.1103/PhysRevLett.125.213902 for (i) details about the intervalley scattering amplitude, (ii) properties of the TCPC, (iii) an all-dielectric TCPC, and (iv) a comparison of the TCPC with conventional cavities.
[30] J. K. Asbóth, L. Oroszlány, and A. Pályi, *A Short Course on Topological Insulators* (Springer, New York, 2016).
[31] D. M. Pozar, *Microwave Engineering* (Wiley, New Jersey, 2011).
[32] P. Sebbah, O. Legrand, and A. Z. Genack, Phys. Rev. E **59**, 2406 (1999).
[33] K. Lai, T. Ma, X. Bo, S. Anlage, and G. Shvets, Sci. Rep. **6**, 28453 (2016).
[34] Z. Gao, H. Xu, F. Gao, Y. Zhang, Y. Luo, and B. Zhang, Phys. Rev. Applied **9**, 044019 (2018).
[35] W. Bogaerts, P. De Heyn, T. Van Vaerenbergh, K. De Vos, S. Kumar Selvaraja, T. Claes, P. Dumon, P. Bienstman, D. Van Thourhout, and R. Baets, Laser Photonics Rev. **6**, 47 (2012).

[36] J. Mork, Y. Chen, and M. Heuck, Phys. Rev. Lett. **113**, 163901 (2014).
[37] Y. Yu, W. Xue, E. Semenova, K. Yvind, and J. Mork, Nat. Photonics **11**, 81 (2017).
[38] W.-P. Su, J. R. Schrieffer, and A. J. Heeger, Phys. Rev. Lett. **42**, 1698 (1979).
[39] M. Xiao, Z. Q. Zhang, and C. T. Chan, Phys. Rev. X **4**, 021017 (2014).
[40] P. St-Jean, V. Goblot, E. Galopin, A. Lemaître, T. Ozawa, L. Le Gratiet, I. Sagnes, J. Bloch, and A. Amo, Nat. Photonics **11**, 651 (2017).
[41] M. Z. Hasan and C. L. Kane, Rev. Mod. Phys. **82**, 3045 (2010).
[42] D. Xiao, M.-C. Chang, and Q. Niu, Rev. Mod. Phys. **82**, 1959 (2010).
[43] M. A. Green, Sol. Energy Mater. Sol. Cells **92**, 1305 (2008).
[44] S. A. Mann, D. L. Sounas, and A. Alù, Optica **6**, 104 (2019).
[45] S. A. H. Gangaraj and F. Monticone, Optica **6**, 1158 (2019).
[46] S. Buddhiraju, Y. Shi, A. Song, C. Wojcik, M. Minkov, I. A. D. Williamson, A. Dutt, and S. Fan, Nat. Commun. **11**, 674 (2020).
[47] K. L. Tsakmakidis, L. Shen, S. A. Schulz, X. Zheng, J. Upham, X. Deng, H. Altug, A. F. Vakakis, and R. W. Boyd, Science **356**, 1260 (2017).
[48] H. A. Haus, *Waves and Fields in Optoelectronics* (Prentice Hall, Englewood Cliffs, NJ, 1984).
[49] S. Fan, W. Suh, and J. D. Joannopoulos, J. Opt. Soc. Am. A **20**, 569 (2003).
[50] W. Suh, Z. Wang, and S. Fan, IEEE J. Quantum Electron. **40**, 1511 (2004).
[51] Y. Yang, Y. Yamagami, X. Yu, P. Pitchappa, J. Webber, B. Zhang, M. Fujita, T. Nagatsuma, and R. Singh, Nat. Photonics **14**, 446 (2020).
[52] J. Perczel, J. Borregaard, D. E. Chang, S. F. Yelin, and M. D. Lukin, Phys. Rev. Lett. **124**, 083603 (2020).
[53] T. Stav, A. Faerman, E. Maguid, D. Oren, V. Kleiner, E. Hasman, and M. Segev, Science **361**, 1101 (2018).
[54] S. Barik, A. Karasahin, C. Flower, T. Cai, H. Miyake, W. DeGottardi, M. Hafezi, and E. Waks, Science **359**, 666 (2018).
[55] M. I. Stockman, Phys. Rev. Lett. **93**, 137404 (2004).